SKA1-LOW CONFIGURATION

Document number SKA-SCI-LOW-001
Context ..... PPP-PPP-PPP-TTT
Revision ..... A
Author ..... SKAO Science Team
Date 2015-10-28
Document Classification ..... UNRESTRICTED
Status ..... Draft

Name	Designation	Affiliation	Signature	
Authored by:				
			Date:	2015-10-28
Owned by:				
			Date:	
Approved by:				
			Date:	
Released by:				
			Date:	

DOCUMENT HISTORY

Revision	Date Of Issue	Engineering Change Number	Comments
A	2014-11-26	-	First draft release for internal review

DOCUMENT SOFTWARE

	Package	Version	Filename
Wordprocessor	MsWord	Word 2007	SKA-TEL-SKO-0000000-C_GenDocTemplate
Block diagrams			
Other			

ORGANISATION DETAILS

Name	SKA Organisation
Registered Address	Jodrell Bank Observatory Lower Withington Macclesfield Cheshire SK11 9DL United Kingdom Registered in England & Wales Company Number: 07881918
Fax.	+44 (0)161 306 9600
Website	www.skatelescope.org

TABLE OF CONTENTS

LIST OF FIGURES

LIST OF TABLES

LIST OF ABBREVIATIONS

AIP ..... Advanced Instrumentation Programme
BD ..... SKA1 Baseline Design
CMB ..... Cosmic Microwave Background
DM..... Dispersion Measure
EMI..... Electromagnetic Interference
EoR ..... Epoch of Reionisation
FoV..... Field of View
FRB ..... Fast Radio Burst
FWHM ..... Full Width Half Maximum
HPSO ..... High Priority Science Objective
ISW ..... Integrated Sachs Wolfe effect
LOFAR ..... LOw Frequency ARray
NIP ..... Non-image Processing
PSF ..... Point Spread Function
RFI ..... Radio Frequency Interference
RM..... Rotation Measure
RMS ..... Root Mean Square
SEFD..... System Equivalent Flux Density
SKA ..... Square Kilometre Array
SKAO ..... SKA Organisation
SCI_REQ- ..... Specification number in this document
TAB ..... Tied Array Beam
VLBI ..... Very Long Baseline Interferometry

1 Introduction

1.1 Purpose of the document

This document is intended to document the considerations in arriving at an array configuration for the SKA1-LOW deployment.

1.2 Scope of the document

The document begins by outlining some of the scientific and technical boundary conditions relevant to the configuration. Based on these considerations, a solution is identified that best satisfies the constraints. The imaging performance of this solution is briefly summarised.

2 References

2.1 Applicable documents

The following documents are applicable to the extent stated herein. In the event of conflict between the contents of the applicable documents and this document, **the applicable documents** shall take precedence.

[AD1]

2.2 Reference documents

The following documents are referenced in this document. In the event of conflict between the contents of the referenced documents and this document, **this document** shall take precedence.

[RD1] SKA-SCI-PRI-002-AppendixA, SKA1 Science Priority Outcomes
[RD2] SKA1 Science Book
[RD3] SKA-XXXXXXXXXXXXXXXX, SKA Phase 1 Science (Level 0) Requirements
[RD4] SKA-XXXXXXXXXXXXXXXX, SKA Baseline Design v 1
[RD5] SKA-XXXXXXXXXXXXXXXX, SKA1 Configurations
[RD6] Mellema, G. et al. 2012, European SKA EoR SWG White Paper
[RD7] Wijnholds, S. and Bregman, J. 2014, Calibratability by Design for SKA's LFAA
[RD8] Trott, C. 2015, "Impact on EoR Power Spectrum of Calibration of Ionospheric Parameters for SKA1-LOW", 25/09/2015
[RD9] SKA-TEL-INAU-0000042, Draft Cost Report
[RD10] Braun, R. 2013, A&A 551, 91, "Understanding synthesis imaging dynamic range"
[RD11] Yatawatta, S., 2013, LOFAR far sidelobe beam gain fluctuations.
[RD12] Wijnholds, S. and Bregman, J., 2015, LFAA Configuration considerations for the inner area of SKA-LOW
[RD13] SKA1 Imaging Performance memo.
[RD14] SKA-XXXXXXXXXXXXXXXX, SKA Phase 1 Level 1 Requirements

3 Scientific Considerations

3.1 High Priority Objectives

The outcome of the Science Prioritisation process [RD1] is a list of thirteen scientific objectives that were assessed as having the highest priority for guiding the design of the SKA1 deployment. Four of the objectives in this list make use of SKA1-LOW. These are considered in turn below. A broader range of objectives is considered subsequently.

3.1.1 EoR – Imaging

Imaging of HI structures at redshifts that span the epoch of reionisation is an extremely technically challenging goal. Current simulations suggest that features with peak brightness temperatures of about 10 mK might be present on 1 - 10 arcmin scales over 1 MHz bandwidth intervals in the frequency range 100 – 200 MHz. Ideally, the instantaneous station field-of-view would be larger than about four square degrees so as to adequately sample one degree angular scales within each pointing [RD6]. Direct imaging of such features will require:

1. The highest possible brightness sensitivity, and,
2. The capability to accurately model and subtract foreground continuum emission.

These requirements lead to the need for:

a. The highest possible surface filling factor of *both* the aperture array stations and the configuration of the stations (for high brightness sensitivity)
b. Exquisite instrumental calibration (in all its forms, for accurate foreground subtraction)
c. Exquisite source modelling (for accurate foreground subtraction).

The most significant calibration challenges are likely to be (i) ionospheric phase fluctuations and (ii) direction dependent gain calibration. Risk mitigation strategies for ionospheric calibration include deployment of the most complete possible instantaneous sampling of the configuration aperture plane. Risk mitigation for the complexities and computational load of direction dependent gain calibration includes deployment of the largest possible station size so as to limit both the all-sky receptivity of the station beam power pattern and the main beam field-of-view. Restriction of the main beam field-of-view is understood to be in direct tension with the scientific desire for simultaneous imaging of a large field. Accurate source modelling requires high sensitivity to the spatial scales that characterise the foreground source population. In the case of the discrete extragalactic continuum source population within a random field of 20 deg^2 area, the power is concentrated on angular scales of 3 – 30 arcsec [RD10]. At 140 MHz, this corresponds to baseline lengths of about 14 – 140 km. In the case of the diffuse Galactic foreground at high latitude, the power is concentrated on the largest scales, > 1 deg, ie. baselines < 150 m that also include the need for total power and very short baseline (< 10m) measurements that are essential to permit a distinction to be made between true emission and possible absorption features.

3.1.2 EoR – Power Spectra

Large area surveys covering 50 – 200 MHz are desired to statistically detect the brightness fluctuations associated with HI in both absorption (expected below 100 MHz) and emission (expected above 100 MHz) relative to the CMB. Ideally, the instantaneous station field-of-view would be larger than about 16 square degrees so as to adequately sample two degree angular scales within each pointing [RD6]. Similar to the direct imaging application outlined above, such observations will require (1) the highest possible brightness sensitivity and (2) the capability to accurately model and subtract foreground continuum emission. These are enabled, as above, by a high filling factor together with excellent calibration and foreground source modelling respectively.

3.1.3 Pulsar Searching

Pulsar searching benefits from the most centrally concentrated collecting area that can be realised. This is fully consistent with the need for the highest possible brightness sensitivity noted previously for the EoR application. In this way, the highest sensitivity can be achieved in conjunction with the broadest possible tied array beams (TABs) so as to maximise the pulsar search speed with a finite number of TABs. The survey speed for pulsar searching also depends on the effective field of view, ie. the product of the station FoV (which scales inversely with diameter squared) with the number of station beams. We will assume that the effective FoV is invariant with station size, since the computational load remains similar for a fixed antenna filling factor; ie. a smaller number of large stations can be used with a larger number of simultaneous station beams. However, there are implications for both the data transmission capacity as well as the beam-forming architecture that will introduce practical limitations on such a trade-off.

3.1.4 Pulsar Timing

Pulsar timing observations also benefit from a high degree of central concentration of the configuration, although in this case a larger fraction of the complete array sensitivity can be utilised since the TAB size is no longer constrained to be large. The limit on TAB sensitivity is determined by the radius out to which real-time calibration is sufficient to allow coherent summation of the station responses. Under nominal conditions this limiting radius for real-time coherent summation is specified to be about 10 km [RD14].

3.2 Additional Objectives

A wide range of additional scientific objectives utilising SKA1-LOW have been documented in both the Science Prioritisation document [RD1] as well as in the SKA Science Book [RD2]. These are enabled by both imaging and non-imaging observational modes.

3.2.1 Imaging Observations

Imaging observations are desired at all frequencies within the SKA1-LOW range of 50 – 350 MHz. Target resolutions vary with the application and span the range of < 10 arcsec to about 200 arcsec. The highest possible sensitivity and synthesized beam quality are desired at each target resolution. Deep continuum and HI absorption applications would benefit from even higher angular resolution than that foreseen in the SKA1 deployment while achieving excellent PSF quality. High brightness sensitivity and PSF quality are desired for the study of diffuse sources, such as galaxy cluster halos and relics as well as cosmic web filaments between galaxy clusters. The most diffuse target sources would benefit significantly from direct interferometric measurement of very short baselines (≤ 10m).

3.2.2 Non-Imaging Observations

Non-imaging observations in both search and targeted modes are desired for a variety of transient phenomena. A goal is to search for these transient signals at all times, commensally, as much as practical. Similar considerations to those already outlined above for Pulsars will apply here.

4 Summary of Configuration Constraints

A consistent set of requirements on the SKA1-LOW configuration arises from both the High Priority and the Additional Science Objectives.

1. The highest possible filling factor of both individual stations and the core configuration over the key frequency interval of 100 – 200 MHz.
2. Instantaneous field-of-view that exceeds about 4 deg^2 for EoR imaging and 16 deg^2 for EoR power spectra (both apply to the frequency range 50 – 200 MHz).
3. Ability to provide excellent quality of ionospheric calibration.
4. Ability to provide excellent quality of direction dependent gain calibration.
5. High sensitivity and good visibility sampling to angular scales of about 10 to 1000 arcsec.

Subsequently, several practical constraints will also be considered, namely:

6. Site-specific and maintenance constraints.
7. Infrastructure Cost.

Each of these constraints will be considered briefly in turn.

4.1 High Filling Factor

The antenna design adopted for SKA1-LOW is a log periodic dipole that provides frequency coverage of 50 – 350 MHz from each antenna. Above the nominal frequency, at which the inter-antenna spacing is about a half wavelength, the effective filling factor of each station will decline as frequency squared. Below the nominal frequency the filling factor remains unity, although the effective aperture of each antenna also remains fixed (rather than varying as ν^{-2} in the sparse regime). For a nominal frequency of about 100 MHz, the filling factor will decline to 0.25 at 200 MHz, limiting the brightness sensitivity that can be achieved in even the most tightly packed of station configurations. A decline to 0.25 is likely to be the largest acceptable degradation of brightness sensitivity within the key frequency interval, suggesting that the nominal frequency should not be lower than about 100 MHz. Even this choice comes with a significant penalty in brightness sensitivity performance at the higher frequencies. RD12 have shown that the brightness temperature sensitivity at a fixed angular scale is degraded as the square root of the inter-antenna spacing; ie. a doubling of the inter-antenna spacing would imply a doubling of the necessary integration time to achieve the same brightness sensitivity. Similarly, the filling factor of stations within the core of the array must be as high as practical since this directly impacts the brightness temperature sensitivity that can be achieved.

4.2 Instantaneous Field-of-view

The desire for a station FWHM beam size > 2 degree for EoR imaging implies a station size (evaluated at 140 MHz) of less than about 62m, while for EoR power spectra, a station size that is smaller by a factor of two, or about 30m, is desired. Other science applications are not directly impacted by the station beam size, provided it exceeds about 1 degree. As noted previously, once the filling factor of antennas within a station has been fixed, the effective field of view of the system can be assumed (to first order) to be invariant with the station diameter, since a larger number of station beams can offset a smaller station beam size at a similar computational load (although constrained by the data transmission and beam-forming architecture). An indirect impact of the station size choice is a limitation on the smallest (projected) baseline that can be measured interferometrically. A practical upper limit on the zenith angle of 45 deg provides only a 30% reduction of the projected baseline relative to the minimum horizontal separation of about one station diameter.

4.3 Ionospheric Calibration

Characterisation of the ionosphere is best accomplished with good instantaneous sampling of the aperture plane with high sensitivity over the entire physical extent of the array configuration. This is used to provide sufficient pierce points of the ionosphere toward calibration sources distributed over the entire station beam field of view. Both analytic estimates [RD7] and numerical simulations [RD8] suggest that 40 to 50 remote station locations are needed to provide a sufficient aperture sampling of a 2D configuration of 70km diameter. The ideal sampling pattern of the aperture would be a uniform random distribution. Previous SKA1 configuration work [RD5] had explored distorted logarithmic spiral configurations outside of a dense core. Preliminary costing studies [RD9] indicate that a randomised distribution on the 70km scale lead to a significant increase of infrastructure costs relative to the distorted logarithmic spiral approach (log-spiral hereafter). The ionospheric calibration performance of the log-spiral configuration is compared with that of various randomised configurations in RD8. A significant difference between these configurations is that the log-spiral approach makes use of a cluster of small stations at each of the remote sites, while all of the random configurations considered make use of only a single small station at each remote site. RD8 conclude that the calibration precision of the log-spiral configuration (re-scaled to be consistent with the current SKA1-LOW scope and described in detail below) is superior to all of the random configurations for observing frequencies between about 50 and 200 MHz. The smaller number of ionospheric pierce points is more than compensated by a higher degree of calibration precision for the log-spiral array. Only at higher frequencies (250 MHz) was marginally superior calibration performance provided by the 50 remote station random variant.

4.4 Direction Dependent Gain Calibration

Self-calibration is required to solve for the time-variable gain toward bright sources both inside as well as outside of the station FoV. The time variability arises from both the ionosphere (discussed above) with a typical timescale of 10 sec and the instrumental response; specifically the detailed polarimetric station beam model that will typically require updating on 10 min timescales for sources inside the station beam. For sources located in the far sidelobe portion of the station beam, the gain updates will be essentially uncorrelated even on 1 sec timescales since neither the ionospheric model nor the beam model will have useful predictive power. Experience with LOFAR [RD7] suggests that only a very limited number of sources in this far-sidelobe regime, about 50, can be accommodated within the calibration strategy due to both the extreme computational cost and ultimately, an inadequate ratio of constraints to unknowns. This places strong requirements on the far sidelobe response pattern of the station beam. RD7 indicate that an RMS far sidelobe level of about -47 dB is needed to keep calibration manageable. They state that it is only necessary to achieve this level when averaged over *all* visibilities. RD10, on the other hand, draw attention to the consequence of the far sidelobe level that applies to *individual* visibilities, since this will degrade the self-calibration precision and therefore the image noise due to all sources, including those within the main beam. Actual measurements of the LOFAR cross-correlation gain fluctuations [RD11] demonstrate that a -24 dB RMS far sidelobe level is achieved in practise for frequencies of 115 – 164 MHz, despite making use of different relative orientations of the antennas in all LOFAR stations (of 31m diameter). The -24 dB RMS value is fully consistent with the physical optics expectation for a far sidelobe level of $\varepsilon_F \approx \eta_F (\lambda/D)^2$, where η_F is of order unity. Significant reduction of the far sidelobe response at these low frequencies can only be achieved with a larger station diameter. Any tapering of the station aperture will only increase, rather than decrease the far sidelobe response in this regime, where the diameter is only a small number of wavelengths. A larger station size also reduces the calibration risk for sources located inside the station beam. As noted in RD12, the computational cost of SKA1-LOW gridding operations, which form an integral part of the self-calibration and imaging cycle, scale inversely as the *station diameter to the sixth power*.

4.5 High sensitivity and good visibility sampling to scales of 10 – 1000 arcsec

Provision of high sensitivity and good sampling over a wide range of angular scales is most effectively achieved through deployment of a "scale-free" distribution of collecting area as function of scale. The most common implementation makes use of a logarithmic spiral distribution with radius, employing a prime number of spiral arms (to eliminate 180 degree rotation symmetry) and a relatively tight winding (to maximise instantaneous azimuthal sampling). The required range of angular scales corresponds to baselines of 0.7 to 70 km at a nominal frequency of 140 MHz.

4.6 Site-Specific and Maintenance Constraints

The SKA1-LOW configuration within Western Australia will be constrained by the boundaries of the currently acquired Boolardy station, as depicted in Figure 2. Moreover, an extensive survey of geophysical and other factors has already been undertaken that provide further restrictions on viable station sites. These additional constraints are also shown in the right hand panel of Figure 2. An important constraint relates to the core location of the configuration. A large, flat, contiguous area is needed that has a sufficiently large separation from the ASKAP site (as discussed in RD5) to limit EMI between these two systems. The core location shown in Figure 2 is the most centrally located one within the Boolardy property that satisfies these requirements.
The detailed station and array configuration design will also need to take relevant operational constraints into account. A first iteration at tabulating those constraints has been prepared by the SKA Operations Team and is included in this document as Appendix C. The constraints relate primarily to the dimensions of access corridors to the deployed equipment on various scales. The requirement (ID2) for an access corridor of one metre minimum width to all antennas is in serious tension with the requirement for maximising the station filling factor, and hence brightness sensitivity. Access requirements on larger scales, a 2.5m separation of station or configuration structures that are larger than 50m, will be more straightforward to satisfy.

4.7 Infrastructure Costs

An important consideration will be the cost of developing and connecting (for data and power transmission) a significant number of remote locations. The major factors contributing to the infrastructure cost are (a) the total number of remote sites to be developed, and (b) the length of connections between them. Both of these factors need to be kept as small as possible, while providing an adequate level of scientific performance.

5 Recommended Reference Configuration

In this section we will provide a recommended array configuration, for which the coordinates are provided in Appendix D. Many aspects of the array configuration follow directly from the summary of constraints presented in Sec.4.

- Individual stations should have a high filling factor of antennas tied to a nominal frequency (the λ/2 antenna spacing) of no lower than about 100 MHz.
- The core configuration of stations should be as tightly packed as practical, while consistent with maintenance requirements (summarised in Appendix C).
- Beyond the tightly packed core, from radii of about 350m to 35km, a logarithmic decline of collecting area with scale is appropriate.
- The total number of extra-core sites and their minimum spanning tree need to be minimised while providing adequate aperture sampling and instantaneous visibility coverage.

The aspect of the configuration that is least well established is the optimum size of each station. Relatively small station sizes are desirable for providing a large contiguous field of view as well as direct interferometric measurement of short baselines, however there is a substantial risk associated with the success of direction dependent gain calibration in this case. The high calibration risk associated with a fixed small station size suggests the use of a risk mitigation strategy based on a variable station size. While complete freedom in station size definition over some specified range might be desirable, the provision of at least three discrete choices would already provide many of the benefits. The specific solution that is proposed is the deployment of a three level hierarchical station design as described in detail in Appendix B.

The smallest unit is a highly filled, 10m sub-station. Six sub-stations, configured as a central unit surrounded by five others form a 30m station. Six stations, configured as one central unit, surrounded by five others form a 90m super-station. Similar super-stations, although each having a distinct overall rotation angle, would be deployed in both the core and on larger scales. An observation could be undertaken with correlation of either the 10m, 30m or 90m units. The choice might depend on the observing frequency, the ionospheric conditions, the scientific application or the available computing capacity, which is likely to evolve with time.

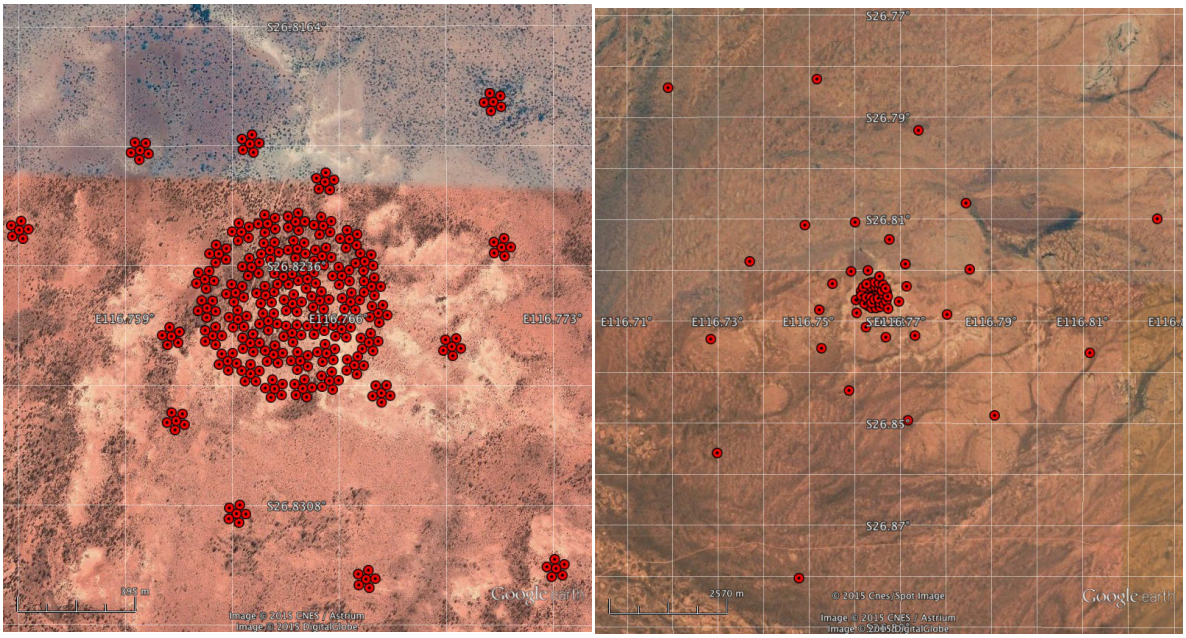

Figure 1: The SKA1-low core (left) and skirt (right). The tightly packed system of randomised concentric rings extends to a radius of about 350m. A tightly wound three arm logarithmic spiral extends between radii of 350m – 6400m.

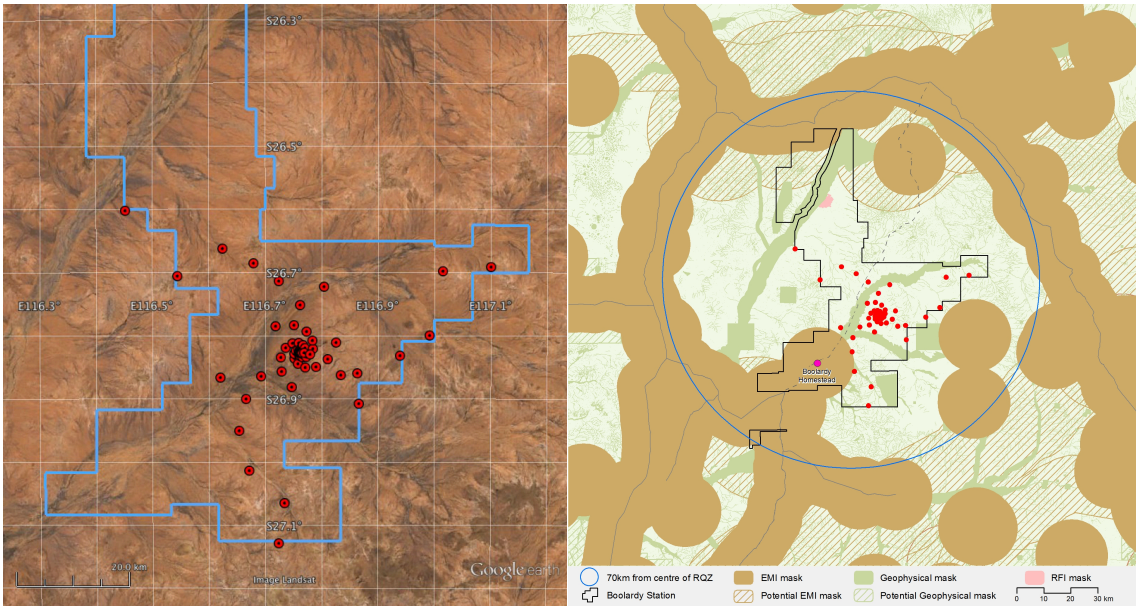

Figure 2: The SKA1-low remote region. A distorted three arm logarithmic spiral extends between radii of 6400m – 35km (left). The configuration is superimposed on the full set of relevant site masks (right).

The array configuration within the core is built up from four concentric, close-packed rings of super-stations, each with a prime number to maximise diversity of visibility sampling and with randomised orientation and placement, yielding a total of 40 super-stations within a circle of 350m radius as illustrated in Figure 1 (left).

A logarithmic density distribution is maintained from 350m to 35km radius, utilising 54 additional super-stations distributed with a three-fold symmetry. A tightly wound (360 deg azimuth sweep) three-arm logarithmic spiral is used at radii of 350m to 6400m where topographic and other site constraints permit this freedom as shown in Figure 1 (right). A more loosely wound, distorted three-arm logarithmic spiral is used at radii beyond 6400m as shown in Figure 2 (left). Distortions of the spiral were introduced with the rotation of super-station triangles of fixed distance from the core. These distortions aimed to maximise the uniformity of the instantaneous aperture sampling while respecting all site constraints and preserving the pattern of radial density decline. An overlay of the complete configuration on the mask of site constraints in given in Figure 2 (right).

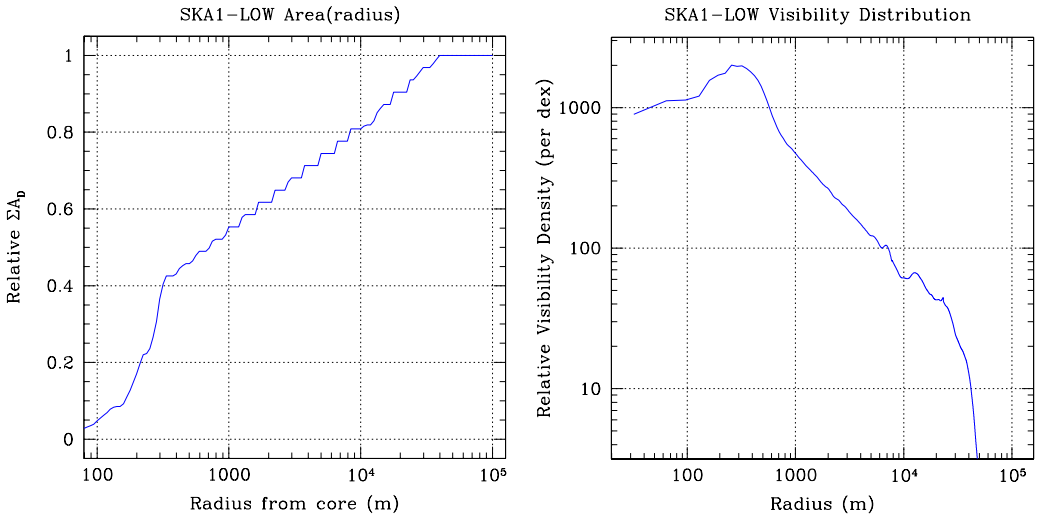

Figure 3: The SKA1-low accumulated collecting area (left) and relative visibility density (right) as function of radius.

The accumulated collecting area as function of radius from the core is illustrated in Figure 3. More than 40% of the collecting area is concentrated within 300m radius and more than 50% within 800m. A smooth, logarithmic build-up of sensitivity over the 300m to 35km radius range is realised, as targeted. The relative density of measured visibilities in a 4h tracking observation at Declination -30 deg is shown in the right-hand panel of Figure 3. We will use the "reference" configuration to designate this recommended approach.

6 Configuration Performance

The visibility sampling of the reference configuration, for both snap-shot and 4-hour tracking observations and for both monochromatic spectral line as well as broad-band continuum (using a 30% fractional bandwidth for illustration) are shown in Figure 4 and 5, for a source at a nominal declination of -30 deg.

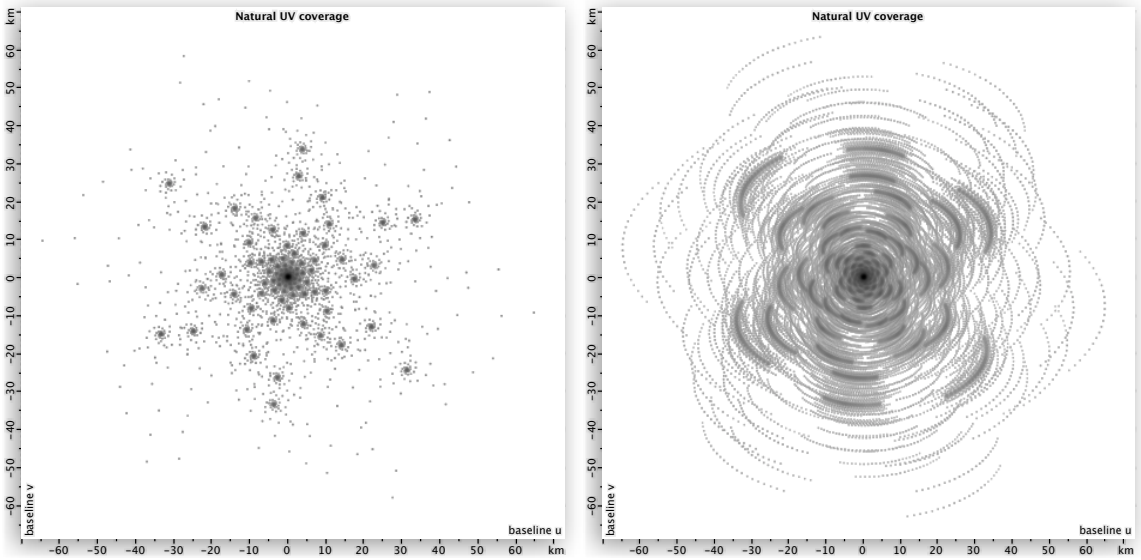

Figure 4: The SKA1-low snap-shot (left) and 4-hour tracking (right) visibility coverage for a monochromatic observation at a nominal declination of -30.

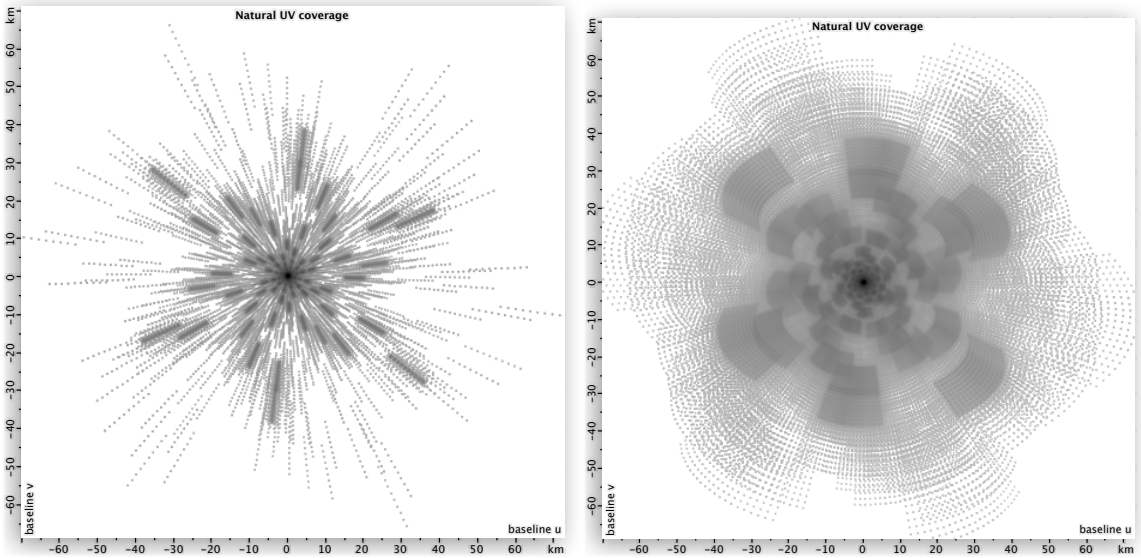

Figure 5: The SKA1-low snap-shot (left) and 4-hour tracking (right) visibility coverage for a broad-band continuum observation (with 30% fractional bandwidth as example) at a nominal declination of -30.

Imaging performance in both monochromatic and broad-band continuum modes of the SKA1-low configuration has been assessed using a set of standardised simulations (that are described in detail in RD13). The resulting performance figures of merit are illustrated in Figure 6. High sensitivity (relative to the natural sensitivity of the entire array) is maintained over a wide range of angular scales, from at least 10 to 1000 arcsec, with the best noise performance achieved at a resolution of 300 arcsec (as seen in the bottom panels). The dirty point spread function quality, measured by the RMS sidelobe level within the central 100 beam areas, is high over a similarly broad range of scales and again is best near 300 arcsec. This is the case for both full 4-hour track observations (middle panels) and transit snap-shot observations (top panels).

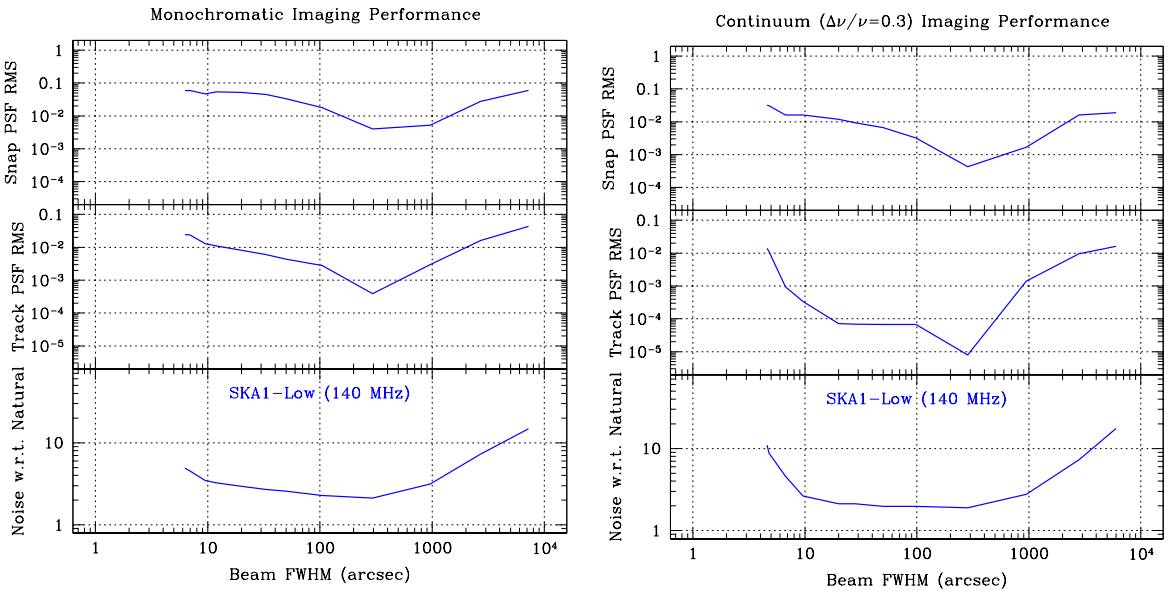

Figure 6: Monochromatic (left hand panel) and broad-band continuum (right hand panel) image noise relative to the total array SEFD (bottom) as well as PSF near-in sidelobe levels for snap-shot (top) and 4-hour track (middle) observations for the SKA1-low configuration as function of required Gaussian beam size at a nominal frequency of 140 MHz.

The Imaging performance can be expressed in physical units by scaling with the array SEFD as function of frequency as specified in the SKA1 Level 1 Engineering requirements [RD14]. Two representative survey strategies are contrasted in Figures 7 (for spectroscopic) and 8 (for broad-band continuum) observations. Outcomes of a wide area survey covering 3π steradians and utilising 2 net years of observing time are illustrated in the left hand panels and those for a single pointing on which 1000 hours of net integration is accumulated in the right hand panels.

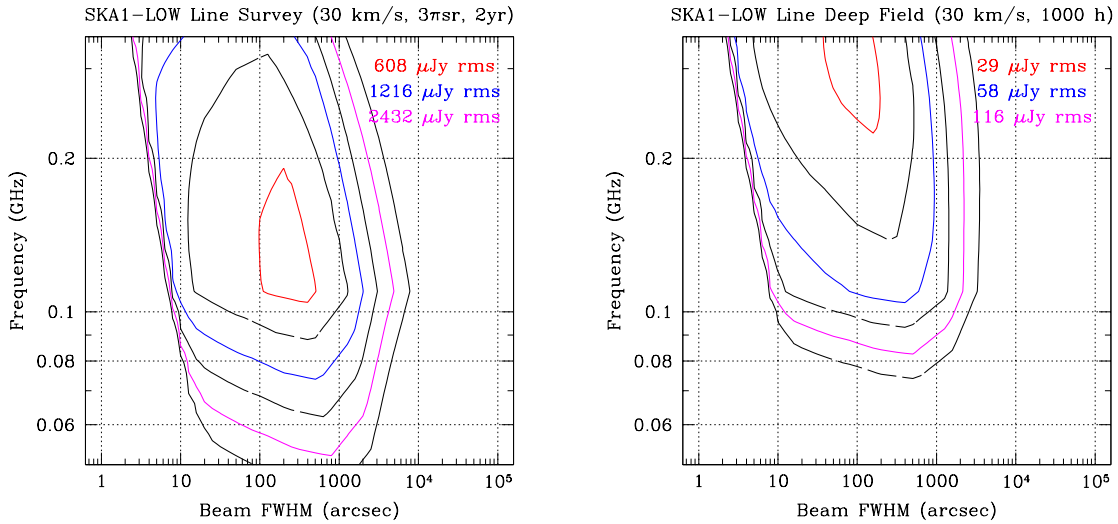

Figure 7: The all-sky survey and deep-field sensitivity performance of SKA1-LOW as function of angular scale and centre frequency for a spectroscopic observation with a channel width of $v_c \times 10^{-4}$.

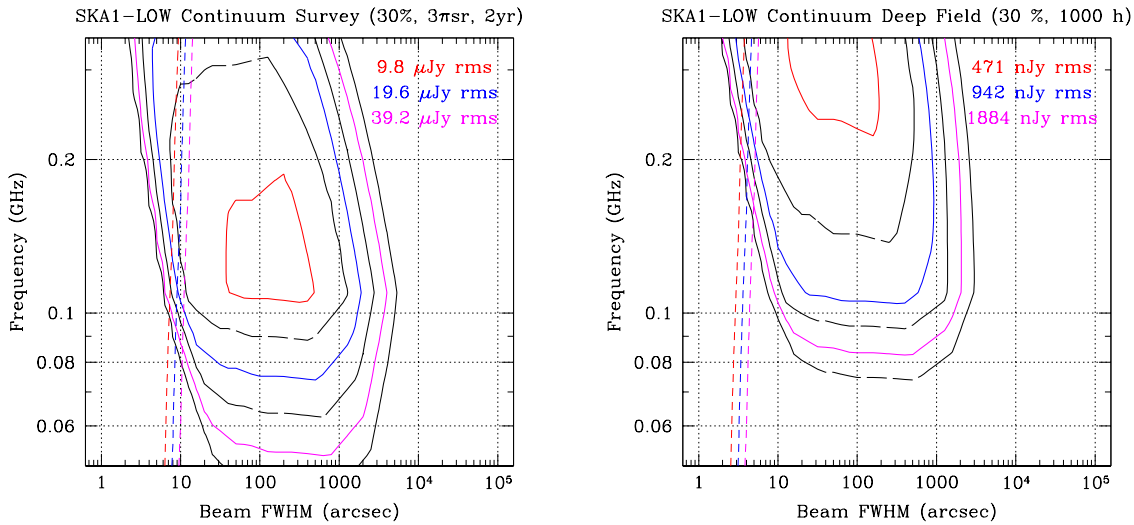

Figure 8: The all-sky survey and deep-field sensitivity performance of SKA1-LOW as function of angular scale and centre frequency for a broad-band continuum observation (30% fractional bandwidth as example). Source confusion levels are indicated by the diagonal dashed contours.

A performance issue of particular relevance is the brightness temperature sensitivity that can be achieved in deep integrations. The RMS brightness sensitivity is plotted as a function of frequency and Gaussian beam size in Figure 11 for 1000 hours of net integration per field at a spectral resolution of 1 MHz, such as might be appropriate for Epoch of Reionisation imaging. MilliKelvin sensitivity can be achieved at resolutions of 300 – 1000 arcsec for frequencies higher than 100 MHz.

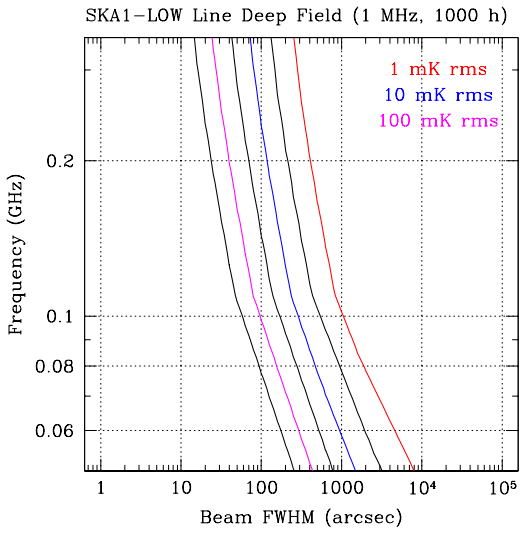

Figure 9: The SKA1-low brightness temperature sensitivity for a deep integration that accumulates 1000 hours of net integration with the reference configuration.

We have also investigated the imaging performance of the reference configuration relative to other approaches, such as the "core plus halo" strategy, whereby only a minimum of collecting area is allocated to a "halo" of remote stations that are uniformly distributed. The "core plus halo" strategy provides somewhat improved sensitivity near 300 arcsec, but also a dramatic loss of performance between 10 and 100 arcsec, as documented in Appendix A. This is likely to constitute a serious impediment to the successful modelling and subtraction of the extragalactic foreground source population needed for EoR experiments. As noted previously, such a strategy also provides inferior ionospheric calibration (as shown in RD8) at the lower frequencies (50 – 200 MHz) needed for the EoR application. And finally, the "core plus halo" approach utilising 45 remote sites represents an increase in the minimum spanning tree over the reference configuration by a factor of 1.7.

7 Appendix A: Performance Comparisons

Some consideration has previously been given to array configurations that attempt to maximise the number of deployed antennas within the core and only deploy some minimum number of stations at remote sites. This class of configuration might be termed a “core plus halo” approach. The ionospheric calibration study of RD8 considers a sequence of such “core plus halo” options that utilise between 10 and 50 randomly placed halo stations in conjunction with a core that holds the remainder. As noted previously, RD8 reach the conclusion that the reference configuration provides superior calibration precision over that of any of the considered “core plus halo” options at low frequencies. The smaller number of ionospheric pierce points being more than compensated with a higher precision measurement at each. Only at 250 MHz do the RD8 simulations suggest that the ionospheric calibration performance of the reference configuration has declined to that of a 50 remote station variant.

Here we also consider more general aspects of the imaging performance. In Figure 10 we compare the array sensitivity and PSF quality, as shown previously in Figure 6, but now contrasted with a “core plus halo” variant with 45 randomly located remote stations, which we will refer to as C+H45.

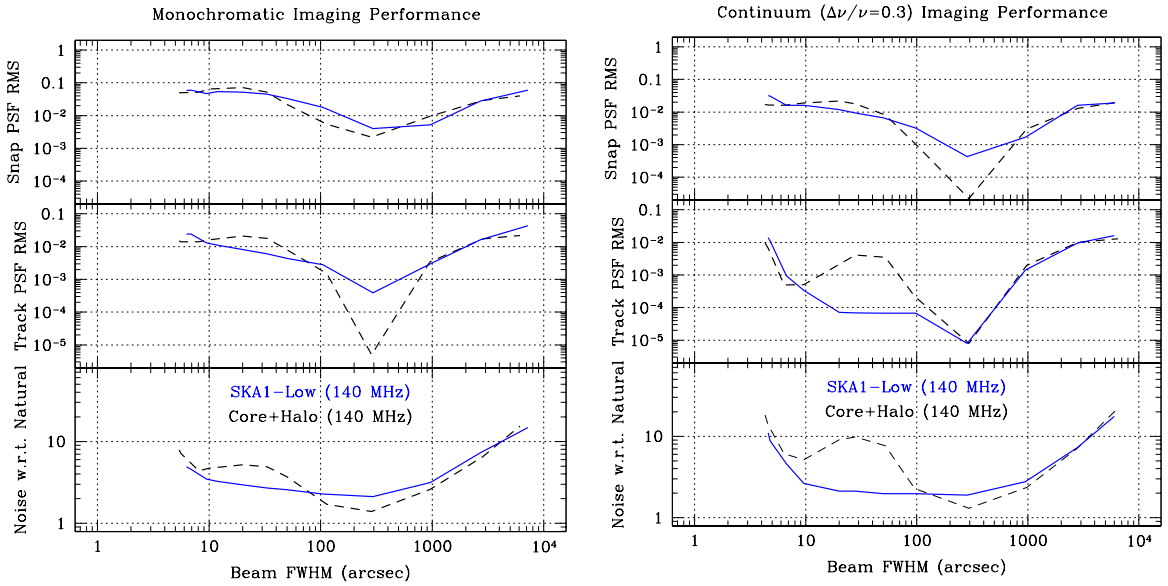

Figure 10: Monochromatic (left hand panel) and broad-band continuum (right hand panel) image noise relative to the total array SEFD (bottom) as well as PSF near-in sidelobe levels for snap-shot (top) and 4-hour track (middle) observations for the reference (solid line) and “core+halo” (dashed line) configurations as function of required Gaussian beam size at a nominal frequency of 140 MHz.

The C+H45 configuration provides somewhat higher sensitivity and PSF quality than the reference configuration at angular scales of about 300 arcsec. However, this comes at the expense of a significant reduction of sensitivity and PSF quality on angular scales of 10 – 100 arcsec. As noted in Section 3.1.1, these are vital angular scales for characterising the extragalactic continuum foreground sources that will require modelling and excision during EoR imaging.

The brightness temperature sensitivity in a deep field observation (as previously shown in Figure 9) is shown for the C+H45 configuration in Figure 11. Since the differences between Figures 9 and 11 are quite subtle, we provide the numerical comparison in Table 1 of the angular resolution at which a brightness temperature RMS sensitivity of 1 mK is achieved for both the C+H45 and the Reference configuration. This reference sensitivity is achieved at a slightly reduced beam size (10 – 15%) for the C+H45 configuration.

Frequency (MHz)	Res. @ 1 mK RMS for C+H45 (arcsec)	Res. @ 1 mK for Ref.Cfg. (arcsec)
50	2535	2844
100	635	750
150	500	610
200	485	565
250	485	565

Table 1: Angular resolution at which 1 mK RMS brightness sensitivity is achieved as function of frequency in a 1000 hour integration for the C+H45 and Reference configurations.

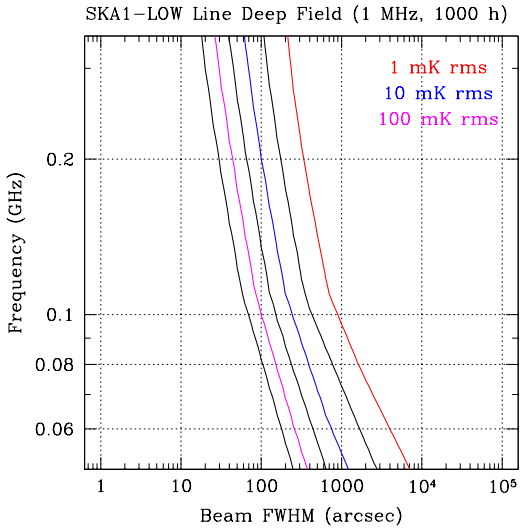

Figure 11: The SKA1-low brightness temperature sensitivity for a deep integration that accumulates 1000 hours of net integration with the C+H45 configuration.

In view of the superior anticipated ionospheric calibration [RD8] and multi-scale imaging quality of the Reference configuration over that of the “core plus halo” variant, while incurring only a minimal degradation of the angular resolution at which the critical EoR brightness sensitivity can be achieved, there is a clear preference for the Reference configuration.

8 Appendix B: Station definition strategy

Inspiration for the design of the SKA1-LOW stations was taken from a local source, namely the Geraldton Wax flower, as depicted in Figure 12. Additional practical guidance on operational constraints is summarised in Appendix C.

Figure 12. The Geraldton Wax flower; a native wildflower of Western Australia.

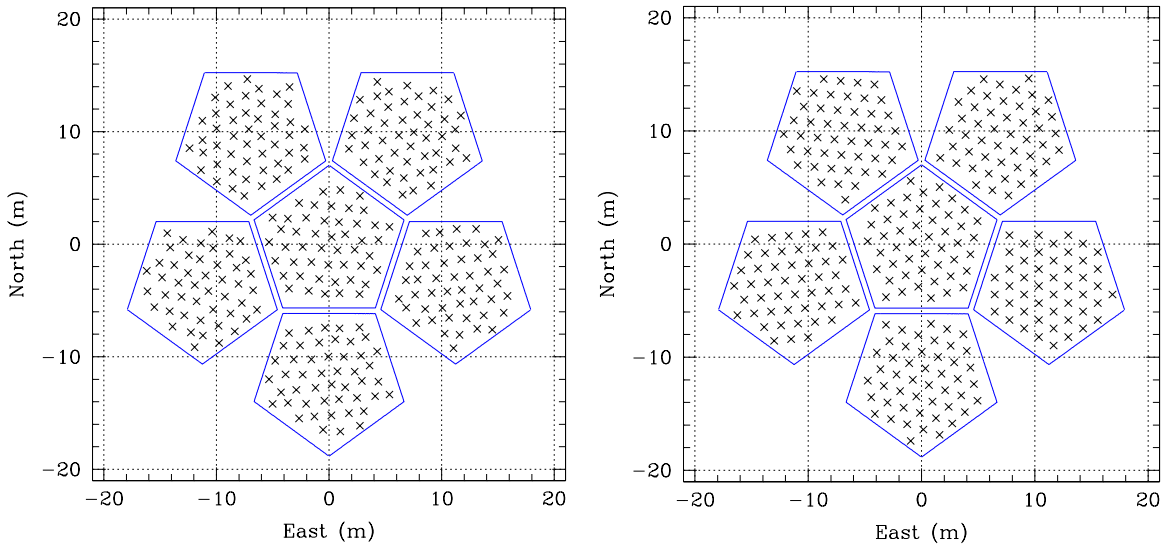

Figure 13. Two possible station layouts. Six similar sub-stations are arranged to form a station, either including randomisation of antenna positions (left) or simply using non-aligned triangular lattices (right).

Production of a multi-level hierarchical station design requires the choice of a basic "tiling" element. Tiling elements should have a prime number of edges/components to eliminate any 180 deg rotation symmetries that will adversely impact the diversity of the aperture sampling that results from correlation with similar structures. The prime number should be as large as possible, but must be smaller than six, since that would result in azimuthal overlap when used in a closely packed configuration. A viable solution is adoption of a regular pentagon tiling as shown in Figure 13.

Each pentagonal sub-station has been populated, in this example, with 48 antennas. The antenna locations have been determined from a triangular sampling lattice, with a fixed mean separation, that is deliberately non-aligned with any of the pentagon edges. Antenna locations are modified with uniform random offsets in two dimensions with a maximum excursion of +/-15% of the mean

separation. Although a mean separation of 1.5m (λ/2 at 100 MHz) is depicted in this example, it is straightforward to rescale all of the illustrated patterns to another mean antenna separation.
When assembling a station from these components, each sub-station is based on a differently aligned triangular sampling lattice. Gaps between the sub-stations have been introduced to restrict mutual coupling effects between sub-stations. The gap spacing can be made as large as necessary to provide isolation at the lowest frequency of interest.

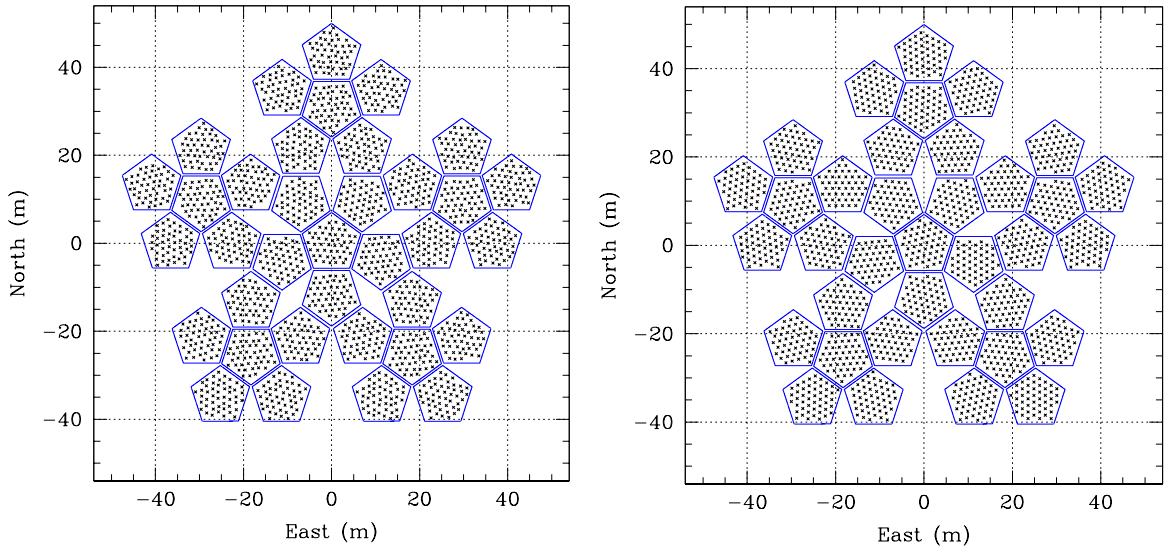

Figure 14. Two possible super-station layouts. Six similar stations are closely packed to form a super-station, either including randomisation of antenna positions (left) or simply using non-aligned triangular lattices (right).

Stations are assembled into a super-station as depicted in Figure 14. A different random antenna realisation is deployed in each of the six stations that together form a super-station. Gaps between the stations are introduced both to restrict mutual coupling effects as well as to provide maintenance access.

The power response patterns at sub-station, station and super-station level of the hierarchy are shown in Figures 15 – 17. The patterns are shown directed toward the zenith and evaluated at 140 MHz for illustration. In each case, both the auto-correlation and a typical cross-correlation power pattern are shown. The cross-correlation is formed with a similar but rotated unit. Peak and median side-lobe levels for all power beams are listed below in Table 2. The auto-correlation pattern at sub-station level (Figure 15 left) clearly shows the residual signature of the triangular sampling lattice at only -3 dB attenuation. The 15% spacing randomisation (while as large as is realistically allowed) cannot erase the basic sampling pattern. Cross-correlation with another orientation of sub-station (Figure 15 right) already provides substantial attenuation of this signature down to -10 dB. Even the station auto-correlation (Figure 16 left) shows significant attenuation of the sampling response. This is similar to the near-in sidelobe level of the station beam (-14 dB). Cross-correlation at the station level (Figure 16 right) improves the residual sampling response to -18 dB and the near-in sidelobes to -16 dB. The super-station auto-correlation (Figure 17 left) yields a residual sampling response of -17 dB and near-in sidelobes of -16 dB while the cross-correlation (Figure 17 right) has -21 dB for the grating response and -18 dB for the near-in sidelobes. These power patterns do not include the additional attenuation, in off-zenith directions, provided by the antenna pattern of each element.

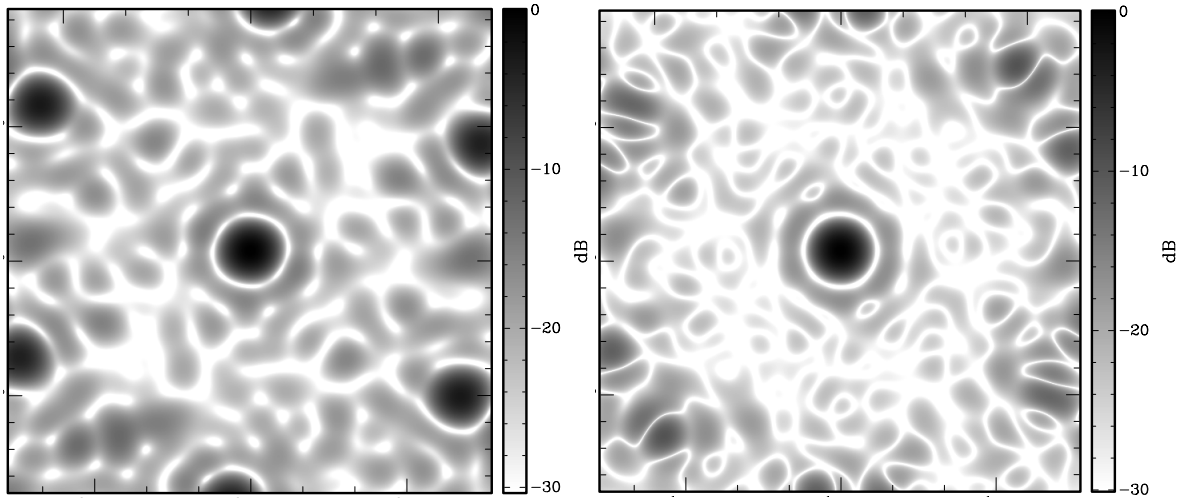

Figure 15. The sub-station power beam with randomisation directed at zenith at 140 MHz both as auto-correlation (left) and typical cross-correlation (right). The top, bottom, left and right edges of the depicted field correspond to the local horizon.

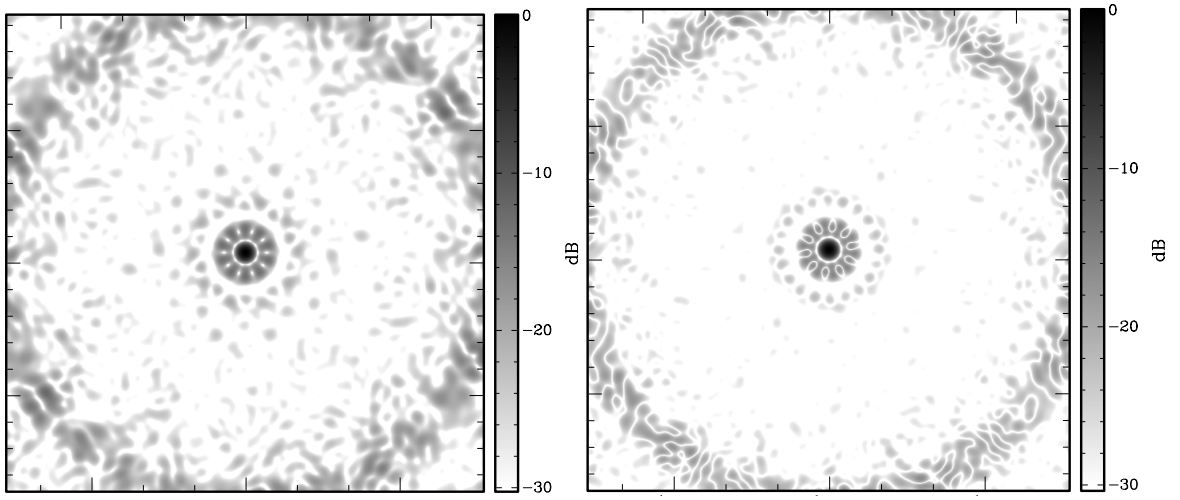

Figure 16. The station power beam with randomisation directed at zenith at 140 MHz both as auto-correlation (left) and typical cross-correlation (right). The top, bottom, left and right edges of the depicted field correspond to the local horizon.

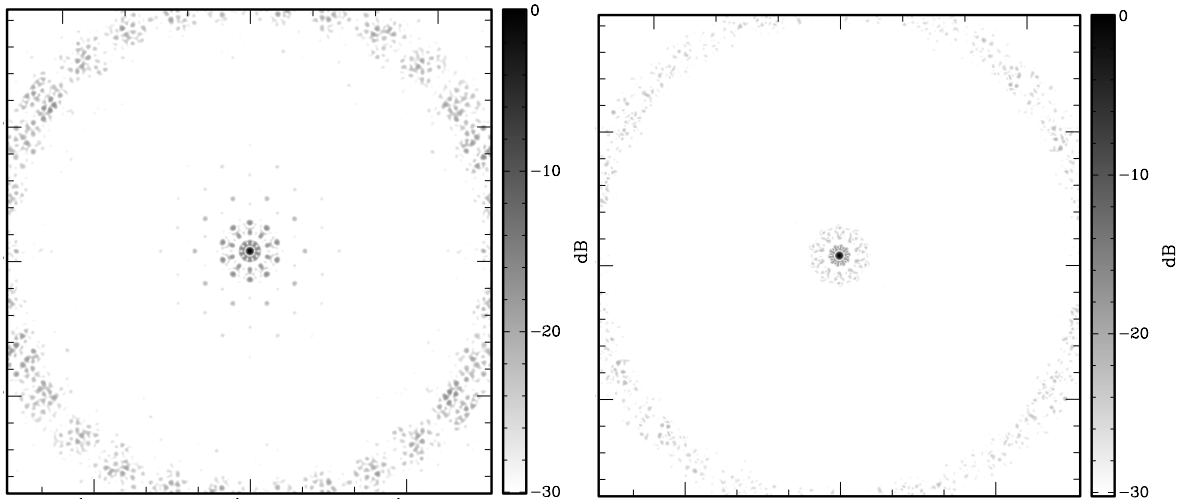

Figure 17. The super-station power beam with randomisation directed at zenith at 140 MHz both as auto-correlation (left) and typical cross-correlation (right). The top, bottom, left and right edges of the depicted field correspond to the local horizon.

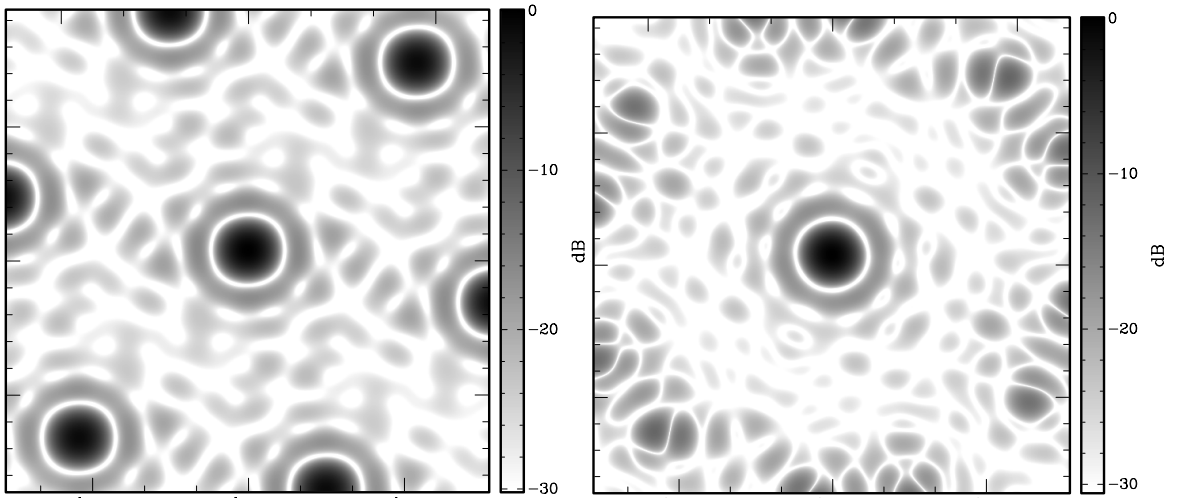

Figure 18. The sub-station power beam with no randomisation directed at zenith at 140 MHz both as auto-correlation (left) and typical cross-correlation (right). The top, bottom, left and right edges of the depicted field correspond to the local horizon.

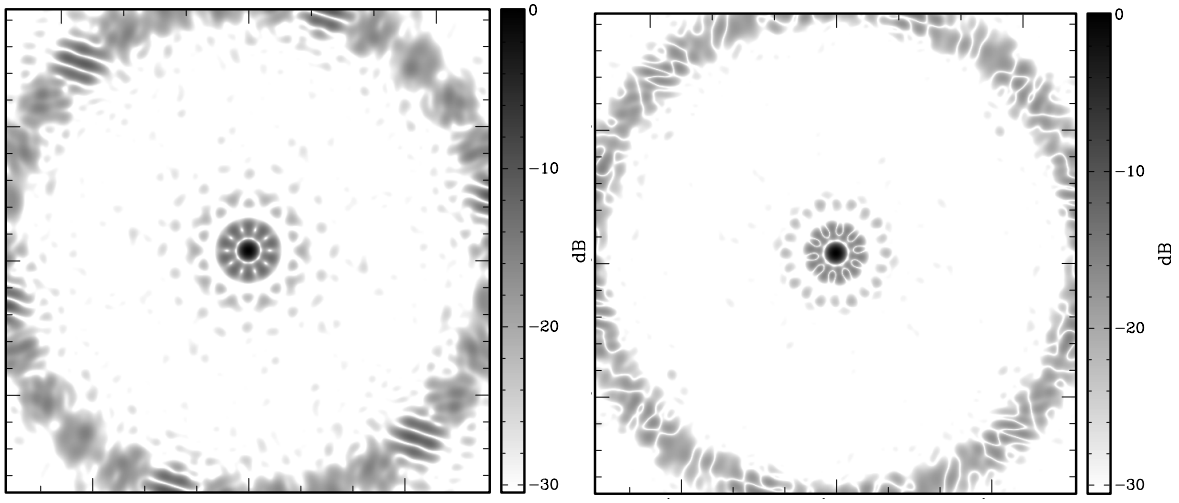

Figure 19. The station power beam with no randomisation directed at zenith at 140 MHz both as auto-correlation (left) and typical cross-correlation (right). The top, bottom, left and right edges of the depicted field correspond to the local horizon.

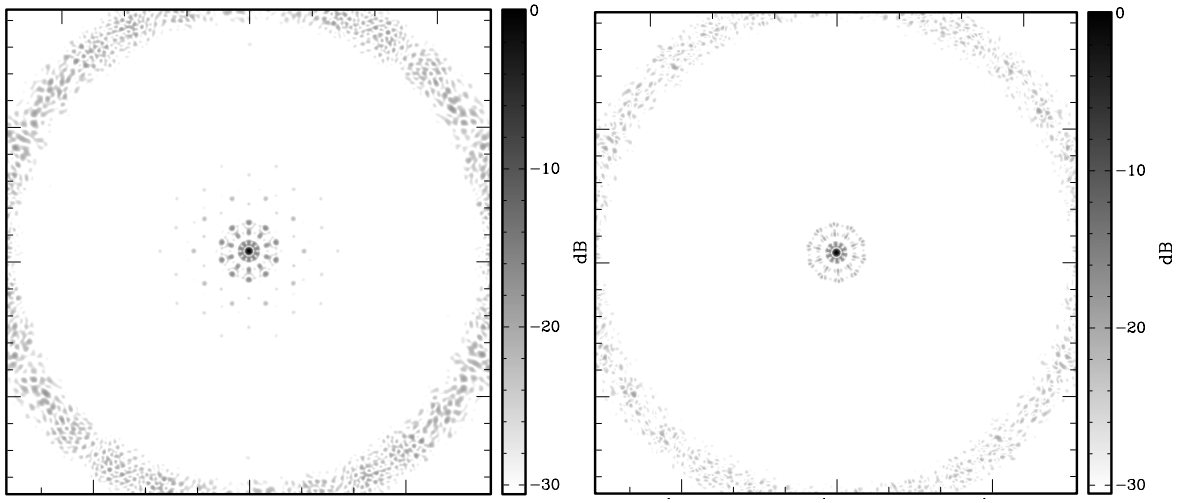

Figure 20. The super-station power beam with no randomisation directed at zenith at 140 MHz both as auto-correlation (left) and typical cross-correlation (right). The top, bottom, left and right edges of the depicted field correspond to the local horizon.

Since there is a recognised tension between the maintenance requirement for a sufficiently wide access corridor to each antenna (Appendix C, ID2) and the scientific requirement for the highest possible filling factor of each station, we have also considered a station layout that does not make use of any randomisation, as shown in the right hand panels of Figures 13 and 14. This would permit the mean antenna separation to be equal to the minimum allowed antenna separation. The sub-station, station and super-station power beams for such non-random layouts are shown in Figures 18 – 20. Non-aligned triangular lattices are used in each sub-station to diversify sampling. The use of non-aligned triangular lattices provides very comparable and in many respects superior sidelobe performance to that of the randomised stations, as demonstrated in Table 2.
Other strategies to provide maintenance access to all antennas, while maximising station filling, such as the use of aperiodic sub-station tiling patterns must still be explored.

Side-lobe Levels (dB)		Random		Non-Ideal		Non-Random		Non-Ideal	
		Auto-	Cross-	Single	Cross Mean	Auto-	Cross-	Single	Cross Mean
Sub-station	near-in peak	-15	-17	-16	-18	-16	-17	-16	-18
	grating peak	-3	-10	-10	-21	-1	-12	-12	-23
	median	-21	-24	-16	-34	-25	-28	-16	-34
Station	near-in peak	-14	-16	-16	-18	-14	-16	-16	-19
	grating peak	-13	-18	-18	-25	-12	-18	-18	-26
	median	-29	-33	-26	-40	-33	-36	-26	-40
Super-station	near-in peak	-16	-18	-18	-20	-16	-17	-17	-18
	grating peak	-17	-21	-21	-33	-19	-19	-19	-34
	median	-38	-41	-35	-45	-42	-45	-35	-45

Table 2: Side-lobe levels of the ideal auto- and cross-correlation power beams illustrated in Figures 15 – 20. Estimates of the non-ideal power side-lobe levels that apply to both single visibilities and to the mean over all power beams in the array are also indicated.

The power patterns at other observing frequencies are simply scaled versions of those shown in Figures 15 – 17 (or 18 – 20). At lower frequencies, the sampling or "grating" response will move outward to below the local horizon, while at higher frequencies this pattern will move inward, ultimately bringing higher multiples of this response, albeit with attenuation by the antenna element pattern, above the horizon.
All of the power patterns shown are geometrically "ideal", in the sense that they do not embody the random complex gain errors and variations that would pertain to a realistic aperture array. As noted previously, the RMS far sidelobe level of real systems is measured to be no better than $\varepsilon_F \approx \eta_F (\lambda/D)^2$, where η_F is of order unity. This should be regarded as an additive term to the patterns shown in Figures 15 – 17 (or 18 – 20), with a magnitude of about -16, -26 and -35 dB for the three different beam-forming scales under consideration. This sidelobe floor is applied to the "non-ideal" columns of Table 2.
None of the station power patterns, even in cross-correlation mode, are expected to provide the RMS far side-lobe level of -47 dB specified by RD7 as necessary to keep the number of far field sources in the calibration solutions manageable. As discussed previously, RD7 suggest that this suppression is only vital in the power pattern response averaged over all visibilities, while RD10 draw attention to the degradation of self-calibration precision resulting from responses within individual visibilities. If the voltage response patterns of the N (sub/super)-stations considered above were independent, then the average cross-power response pattern might be improved by about √N, or

18, 14 and 10 dB (for the sub-station, station or super-station case), over an individual cross-correlation. This improvement in the median sidelobe level is also shown in Table 2, as well as the measured peak near-in and grating sidelobe level achieved in the mean over 94 different orientations of the super-stations. In view of the anticipated gain error contribution to the far sidelobe levels, only the 90m super-station variant looks likely to provide an average power pattern with RMS far side-lobe level that approaches -47 dB.

9 Appendix C: Operational Constraints

From an operational perspective, there will be a need for physical access to the LOW antennas for maintenance and repair. This will constrain the possible solutions for the array configuration. The constraint is encapsulated in the following requirements.

ID	Requirement	Comment
1	Every antenna must be accessible to service personnel.	We can assume personnel will move through each station on foot. The requirement implies that there must be an access route from the outer edge of the station to every antenna. This does not necessarily equate to a minimum centre-to-centre distance for adjacent antennas, but that may be the simplest means of implementing it.
2	The access routes through the station must have a minimum width of 1 m.	This is to allow for easy passage of personnel and equipment, including antennas.
3	The Antenna Power Interface Units (APIUs) must also be accessible to service personnel.	If the APIUs are located at the edges of the stations, this will not be an issue. If they are located in the interior of the stations, then there must be a direct (as opposed to potentially zig-zag) access route from the edge of the station to the APIU.
4	The maximum walking distance from the edge of a station to any antenna should be 25 m.	This is a subjective judgment, but there is a limit to how far personnel should be expected to carry equipment. This requirement is directly related to the size of the stations.
5	All points around the circumference of a station should be accessible by vehicle.	Adjacent stations should be separated by enough space to allow for vehicular access; a minimum separation of 2.5m seems appropriate. (This assumes the stations are sufficiently densely populated that service vehicles cannot move within the interior of a station. If this assumption is incorrect then requirements 4 and 5 will have to be re-phrased.)

10 Appendix D: Station Coordinates

WGS84 coordinates of the 564 stations depicted in Figures 1 and 2 are listed below.

116.7644482	-26.82472208
116.7642355	-26.82492687
116.7645995	-26.82496696
116.764754	-26.82466847
116.7644861	-26.82444427
116.7641654	-26.82460403
116.765363	-26.82463167
116.7651372	-26.82482468
116.7654982	-26.82488381
116.7656719	-26.8245944
116.7654191	-26.82435636
116.7650888	-26.82449848
116.7649503	-26.82398302
116.765169	-26.82378358
116.7648063	-26.82373493
116.7646427	-26.82402893
116.764904	-26.82425967
116.7652289	-26.82410815
116.7641361	-26.82390909
116.763842	-26.82381528
116.7639457	-26.82413049
116.7643119	-26.82413998
116.7644355	-26.82383029
116.764145	-26.82362917
116.7635415	-26.82447089
116.7635166	-26.82419191
116.763238	-26.82440618
116.7633794	-26.82470987
116.7637445	-26.82468334
116.7638292	-26.82436355
116.7636344	-26.82523936
116.7633378	-26.8253251
116.7636334	-26.82551929
116.7639307	-26.82532696
116.7638186	-26.82501382
116.7634521	-26.82501254
116.7644359	-26.82559788
116.7644629	-26.8258768
116.7647399	-26.82566061
116.7645961	-26.8253578
116.7642311	-26.82538669
116.7641488	-26.82570763

116.7652586	-26.82537632
116.7651726	-26.82564522
116.7655173	-26.82553264
116.765504	-26.82520362
116.765151	-26.82511378
116.764947	-26.82538711
116.7636826	-26.82311543
116.7634784	-26.8229042
116.7633954	-26.82322439
116.7637093	-26.82339399
116.7639862	-26.82317893
116.7638435	-26.82287578
116.7630708	-26.82362631
116.7633097	-26.82380626
116.7633353	-26.82347807
116.7629954	-26.82335482
116.7627597	-26.82360689
116.7629543	-26.82388582
116.7625312	-26.82439228
116.7627578	-26.82420036
116.7623979	-26.82413919
116.7622218	-26.82442805
116.7624732	-26.82466697
116.7628045	-26.82452678
116.7626142	-26.82519607
116.7629047	-26.82509374
116.7625957	-26.82491652
116.7623124	-26.82512587
116.7624466	-26.825432
116.7628131	-26.8254117
116.7630254	-26.82590178
116.7627678	-26.82574383
116.762778	-26.82607218
116.7631294	-26.82616557
116.763337	-26.82589459
116.7631144	-26.82563354
116.763809	-26.82625323
116.7641157	-26.82620361
116.763851	-26.82597592
116.7635281	-26.82613151
116.7635935	-26.82645549
116.7639567	-26.82649979
116.7647097	-26.82643909
116.7646107	-26.82670416
116.7649603	-26.82660554

116.7649636	-26.82627684
116.7646163	-26.8261724
116.7643977	-26.82643619
116.765597	-26.82621226
116.7658208	-26.82640728
116.7658726	-26.82608145
116.7655432	-26.82593694
116.7652884	-26.82617293
116.7654598	-26.82646351
116.7661006	-26.82548837
116.7661316	-26.82520974
116.7658148	-26.82537616
116.7658931	-26.82569744
116.7662583	-26.82572989
116.7664055	-26.82542838
116.7664018	-26.82466857
116.7661952	-26.82487807
116.7665599	-26.82490986
116.766706	-26.82460817
116.766432	-26.82439024
116.7661159	-26.8245566
116.7661067	-26.82388258
116.765795	-26.82388909
116.7660174	-26.82415068
116.7663634	-26.82404152
116.7663543	-26.82371247
116.766003	-26.82361892
116.7654454	-26.82329521
116.7657552	-26.82332776
116.7655756	-26.82304085
116.7652162	-26.82310547
116.7651731	-26.82343186
116.765506	-26.82356936
116.7646098	-26.82307981
116.7648403	-26.82289165
116.7644812	-26.82282511
116.7642998	-26.82311048
116.7645463	-26.82335369
116.7648803	-26.82321876
116.7665311	-26.8265699
116.7666146	-26.8268397
116.7668428	-26.82658202
116.7666404	-26.82630787
116.7662871	-26.826396
116.7662715	-26.8267246

116.7670198	-26.82588606
116.767329	-26.82584924
116.767076	-26.82561069
116.7667459	-26.82575273
116.7667938	-26.82607893
116.7671543	-26.82613823
116.7673319	-26.82500836
116.7671223	-26.82480117
116.7670477	-26.82512337
116.7673655	-26.82528633
116.767637	-26.82506556
116.7674866	-26.82476523
116.7671046	-26.82420954
116.766854	-26.82437601
116.7672035	-26.82447491
116.7674165	-26.82420752
116.7671989	-26.82394266
116.7668511	-26.82404637
116.7668786	-26.82345584
116.7668361	-26.82373287
116.767159	-26.82357786
116.767095	-26.82325452
116.7667316	-26.82320926
116.7665714	-26.82350489
116.766363	-26.82278433
116.7666027	-26.82296324
116.7666266	-26.8226347
116.7662855	-26.82251338
116.7660518	-26.82276698
116.7662486	-26.82304478
116.765481	-26.82238501
116.7653566	-26.82264142
116.7657143	-26.82257062
116.7657499	-26.82224296
116.7654135	-26.82211182
116.7651704	-26.82235849
116.7645514	-26.82225816
116.7642949	-26.82209925
116.7643034	-26.82242788
116.7646547	-26.82252201
116.7648631	-26.82225139
116.7646405	-26.82199022
116.763609	-26.82231499
116.7638651	-26.82247454
116.7638576	-26.82214587

116.7635063	-26.82205073
116.7632975	-26.8223207
116.7635185	-26.8225829
116.7627254	-26.82256821
116.762414	-26.82255659
116.7626167	-26.82283048
116.7629695	-26.82274224
116.7629851	-26.82241334
116.7626411	-26.82229879
116.7619663	-26.82322319
116.7618618	-26.82348706
116.7622134	-26.82339368
116.7622234	-26.82306459
116.7618776	-26.82295521
116.7616547	-26.82321592
116.7614953	-26.82398861
116.7612785	-26.82378732
116.7612151	-26.82411125
116.7615389	-26.82426569
116.7618024	-26.82403732
116.7616419	-26.82374158
116.7615668	-26.82485546
116.7615573	-26.82513493
116.7618606	-26.82494982
116.7617575	-26.82463387
116.7613907	-26.82462445
116.7612672	-26.82493399
116.7617594	-26.8256871
116.7615084	-26.82585353
116.7618584	-26.82595233
116.762071	-26.82568444
116.7618526	-26.82542019
116.7615049	-26.82552523
116.7622645	-26.82644426
116.762285	-26.82672346
116.7625667	-26.82651277
116.7624307	-26.82620757
116.762065	-26.82622914
116.7619751	-26.8265481
116.7630336	-26.82682453
116.7627379	-26.82673523
116.7628478	-26.82704922
116.7632146	-26.82705246
116.7633307	-26.82674043
116.7630366	-26.82654477

116.7638436	-26.82727916
116.7637233	-26.82753753
116.7640798	-26.82746149
116.7641103	-26.82713391
116.763772	-26.82700693
116.7635325	-26.82725607
116.7647918	-26.82727244
116.7648507	-26.82699765
116.7645189	-26.82713731
116.7645641	-26.82746351
116.7649241	-26.82752586
116.7651015	-26.82723819
116.7656863	-26.82703741
116.7659975	-26.82702239
116.7657669	-26.82676709
116.7654248	-26.82688516
116.7654444	-26.82721387
116.7657989	-26.82729852
116.7655416	-26.82106055
116.7658457	-26.82099802
116.7655696	-26.82078203
116.7652549	-26.82095087
116.765337	-26.82127159
116.7657022	-26.82130043
116.7630128	-26.81991705
116.7627768	-26.82009999
116.7631341	-26.82017487
116.7633237	-26.81989312
116.7630831	-26.81964448
116.7627454	-26.81977288
116.759302	-26.82010469
116.7591342	-26.81986889
116.7590002	-26.82017481
116.7592833	-26.82038407
116.7595924	-26.82020697
116.7595002	-26.81988845
116.7552218	-26.82250338
116.755289	-26.82223019
116.7549528	-26.82236169
116.7549887	-26.82268926
116.7553471	-26.82275973
116.7555321	-26.8224756
116.7523362	-26.82763219
116.7521755	-26.82739243
116.7520323	-26.82769566

116.7523096	-26.82791102
116.7526239	-26.82774078
116.7525401	-26.82742053
116.7528083	-26.83516376
116.7531201	-26.83516833
116.7529094	-26.83489911
116.7525589	-26.83499588
116.7525535	-26.83532495
116.7529005	-26.83543086
116.7588582	-26.84344023
116.7586482	-26.84364692
116.7590128	-26.8436831
116.7591637	-26.84338326
116.7588922	-26.84316224
116.7585742	-26.84332526
116.7717852	-26.84928846
116.7720649	-26.84941233
116.7720028	-26.84908806
116.7716403	-26.84904091
116.7714778	-26.8493351
116.77174	-26.84956547
116.7907593	-26.84832051
116.7910218	-26.84816925
116.7906802	-26.84804964
116.7904478	-26.84830457
116.7906466	-26.84858159
116.7910009	-26.84849746
116.8116119	-26.83604987
116.8117153	-26.83578614
116.811364	-26.83588009
116.811355	-26.83620874
116.8117006	-26.83631805
116.8119238	-26.83605693
116.8263363	-26.80982597
116.8260718	-26.80967767
116.8260977	-26.81000583
116.8264536	-26.81008543
116.8266471	-26.80980584
116.8264111	-26.80955447
116.7674359	-26.82740253
116.7672459	-26.82718045
116.7671418	-26.82749596
116.7674443	-26.82768232
116.7677349	-26.8274815
116.767612	-26.8271717

116.7698039	-26.82600988
116.77011	-26.82606481
116.7699564	-26.82576599
116.7695925	-26.8258044
116.7695208	-26.82612704
116.7698405	-26.82628757
116.7714777	-26.82303239
116.771567	-26.82276407
116.7712208	-26.82287358
116.7712301	-26.8232024
116.7715818	-26.82329596
116.7717896	-26.82302507
116.7712018	-26.81866239
116.7714415	-26.81848349
116.771086	-26.81840264
116.7708909	-26.81868112
116.7711253	-26.81893348
116.771466	-26.81881146
116.7676921	-26.81385568
116.7673852	-26.8138061
116.7675446	-26.81410199
116.7679078	-26.81405769
116.7679728	-26.81373397
116.7676497	-26.81357848
116.7601905	-26.81046217
116.7599194	-26.81060019
116.7602534	-26.81073609
116.7605003	-26.81049323
116.7603197	-26.8102074
116.7599608	-26.81027311
116.7491797	-26.81102098
116.7494729	-26.81111636
116.7493712	-26.81080027
116.7490048	-26.81078926
116.7488798	-26.81109845
116.7491692	-26.81130039
116.7370678	-26.81813825
116.736996	-26.81841063
116.7373338	-26.81828398
116.7373043	-26.81795585
116.7369477	-26.81787988
116.7367572	-26.81816107
116.7285129	-26.83335554
116.7282171	-26.83344399
116.728515	-26.83363506

116.72881	-26.8334399
116.728694	-26.83312809
116.7283276	-26.83313063
116.7299145	-26.85569231
116.72984	-26.85596376
116.7301795	-26.8558401
116.730153	-26.85551205
116.7297974	-26.85543307
116.7296033	-26.85571211
116.747852	-26.88025298
116.7476383	-26.8804568
116.7480017	-26.8804983
116.7481583	-26.88020113
116.747892	-26.87997543
116.7475701	-26.88013325
116.760367	-26.82570306
116.7605952	-26.82589362
116.7606392	-26.82556698
116.7603066	-26.82542847
116.7600572	-26.82566986
116.760236	-26.82595702
116.7605269	-26.82824005
116.7604889	-26.82851764
116.7608095	-26.82835815
116.7607398	-26.82803559
116.7603759	-26.8279954
116.7602208	-26.8282928
116.762565	-26.83102888
116.7626487	-26.83129814
116.7628766	-26.83104044
116.7626732	-26.83076623
116.7623205	-26.83085524
116.7623049	-26.8311837
116.766921	-26.83299997
116.7672327	-26.83298477
116.767001	-26.83272939
116.766659	-26.8328483
116.766679	-26.83317651
116.7670337	-26.83326112
116.7733133	-26.83267481
116.7730062	-26.8326265
116.7731672	-26.83292203
116.7735303	-26.83287564
116.7735934	-26.83255161
116.7732691	-26.83239769

116.7803428	-26.82854156
116.7806421	-26.82862077
116.7805191	-26.82831103
116.7801525	-26.82831999
116.7800491	-26.82863524
116.7803511	-26.82882135
116.7853107	-26.81970614
116.7854334	-26.81944887
116.7850761	-26.81952167
116.7850429	-26.81984931
116.78538	-26.81997916
116.7856215	-26.81973102
116.7844836	-26.80674243
116.7847901	-26.80669177
116.7845244	-26.80646485
116.784202	-26.80662208
116.7842689	-26.8069453
116.7846324	-26.80698817
116.7740734	-26.79248364
116.7737645	-26.79252148
116.7740178	-26.7927589
116.7743479	-26.79261621
116.7742987	-26.79229037
116.773938	-26.79223162
116.7518181	-26.78241122
116.751959	-26.782661
116.7521263	-26.78236854
116.7518682	-26.78213492
116.7515408	-26.782283
116.7515965	-26.78260788
116.7191563	-26.78406519
116.7192132	-26.78434019
116.7194655	-26.78410137
116.71929	-26.78381233
116.7189299	-26.78387292
116.7188822	-26.78419892
116.8348215	-26.86126618
116.8345555	-26.86141228
116.8348941	-26.86153839
116.8351325	-26.86128829
116.834941	-26.8610077
116.8345845	-26.86108436
116.8640441	-26.85834219
116.8638013	-26.85816637
116.8637826	-26.85849509

116.8641253	-26.85861207
116.8643555	-26.85835623
116.8641553	-26.8580806
116.866757	-26.90649213
116.8666616	-26.90675851
116.8670102	-26.90665596
116.8670088	-26.90632706
116.8666595	-26.90622657
116.866445	-26.906493
116.9397062	-26.8304908
116.9394253	-26.83061244
116.9397486	-26.83076773
116.9400129	-26.83054062
116.9398541	-26.83024436
116.9394904	-26.83028874
116.9922124	-26.79850839
116.992378	-26.79874542
116.9925148	-26.79844012
116.9922336	-26.79822948
116.9919229	-26.79840438
116.9920127	-26.79872316
117.0156842	-26.69695549
117.0153923	-26.6968575
117.0154901	-26.69717422
117.0158565	-26.69718887
117.0159845	-26.69688037
117.0156975	-26.69667593
117.1009158	-26.6902092
117.1010877	-26.68997583
117.100722	-26.68999029
117.1006241	-26.69030715
117.1009291	-26.69048857
117.1012158	-26.69028453
116.6935773	-26.86318025
116.6932814	-26.86326957
116.6935806	-26.86345992
116.6938752	-26.86326399
116.6937581	-26.86295212
116.6933917	-26.86295542
116.6668313	-26.89899684
116.6666746	-26.89875492
116.6665262	-26.89905568
116.6667996	-26.89927517
116.6671168	-26.89910964
116.667039	-26.89878831

116.6213994	-26.86517371
116.6212543	-26.86492586
116.6210918	-26.86522062
116.6213545	-26.86545065
116.6216792	-26.86529756
116.6216169	-26.8649731
116.6546886	-26.9493466
116.6549949	-26.94939995
116.6548396	-26.94910184
116.6544752	-26.94914214
116.654406	-26.94946541
116.6547276	-26.94962419
116.6724653	-27.01234887
116.672553	-27.01208037
116.6722073	-27.01219107
116.672218	-27.01251995
116.6725706	-27.01261221
116.6727773	-27.01234029
116.7349808	-27.06371331
116.7347863	-27.06349417
116.7346883	-27.06381128
116.7349943	-27.0639929
116.7352815	-27.06378848
116.7351533	-27.06348002
116.7247812	-27.12740782
116.7250773	-27.12731787
116.7247774	-27.12712802
116.7244825	-27.12732479
116.7246004	-27.12763606
116.7249677	-27.12763254
116.7626524	-26.75058745
116.7623415	-26.7506028
116.7625726	-26.75085782
116.7629142	-26.7507392
116.762894	-26.75041091
116.7625399	-26.7503267
116.8050883	-26.72161867
116.8051743	-26.7218876
116.8053997	-26.72162821
116.8051945	-26.72135573
116.8048428	-26.72144677
116.8048301	-26.72177563
116.7249139	-26.71273903
116.7251414	-26.71293026
116.7251866	-26.7126037

116.7248545	-26.71246465
116.7246045	-26.71270493
116.7247822	-26.71299274
116.6800382	-26.68453503
116.6803365	-26.6844553
116.6800464	-26.68425514
116.6797449	-26.68444134
116.6798485	-26.68475665
116.6802141	-26.68476573
116.6251905	-26.66137637
116.6254977	-26.66142276
116.6253349	-26.66112852
116.6249728	-26.66117624
116.6249116	-26.66150051
116.6252358	-26.66165316
116.545256	-26.70465642
116.5455122	-26.7048155
116.5455034	-26.70448653
116.5451528	-26.70439266
116.5449447	-26.70466303
116.5451667	-26.7049243
116.4526347	-26.60102013
116.4524856	-26.60126583
116.4528481	-26.60122353
116.452916	-26.60090062
116.4525953	-26.60074255
116.4523287	-26.60096771

Table 3. WGS84 station coordinates.